Applied Acoustics 73 (2012) 234–242

Contents lists available at SciVerse ScienceDirect

Applied Acoustics

journal homepage: www.elsevier.com/locate/apacoust

One dimensional study of a module for active/passive control of both absorption and transmission

Manuel Melon [a,*], Philippe Herzog [b], Azzedine Sitel [c], Marie-Annick Galland [c]

[a] CNAM, LMSSC, 292 rue Saint Martin, F-75141 Paris cedex 3, France
[b] CNRS, LMA, 31 chemin Joseph Aiguier, F-13402 Marseille cedex, France
[c] LMFA, École Centrale de Lyon, F-69134 Écully cedex, France

ARTICLE INFO

Article history:
Received 26 April 2011
Received in revised form 8 September 2011
Accepted 13 September 2011
Available online 8 October 2011

Keywords:
Active control
Hybrid systems
Scattering matrix
Wave propagation in tubes

ABSTRACT

Hybrid active/passive absorbers have proven to be efficient over a large frequency range. The next step consists in building up a system which can exhibit good absorption and insulation properties. To simulate such hybrid cell, active and passive behaviors of an electroacoustic loudspeaker have been modelized by using a one-dimensional approach. The rear acoustic load at the back of the membrane has been taken into account to obtain a reliable model. The proposed model has been validated with measurements performed in a 7 cm diameter tube. Then, a hybrid cell composed of a porous plate and a small thickness loudspeaker has been designed and numerically tested. It is shown that, when driving the loudspeaker for total absorption, the transmission losses are suppressed at lower frequencies. To overcome this problem, a dual actuator cell is designed to deal with both absorption and transmission. Simulations shows that this solution can lead to good results. It is also shown that interaction of the loudspeakers can be significantly reduced by using directive sources, thus lowering supplying voltages and condition number of the matrix inversion required by the control process.

1. Introduction

Many situations involve multiple volumes including sound sources; this is the case of buildings, transportations, hoods, etc. The boundaries of each volume plays a double role: it increases the radiated pressure on the source side, and it transmits part of the acoustic energy on the other side. The design of acoustically efficient walls is therefore a trade-off between both aspects, of course limited by practical constraints such as the resulting cost, thickness and weight.

Usually, walls are optimized for low acoustic transmission, as this is the major challenge in many applications. Passive approaches have been improved over the years, starting from the basic "law of mass" concept to reach multiple-layer designs [1–4]. A very typical example is the partition walls for buildings, involving two sheets of gypsum separated by a fluid layer, with a wide range of possible configurations [5–7]. The basic objective of such designs is to reduce the vibration of the receiver side of the wall, ideally leading to a perfectly motionless boundary.

Other applications consider absorption as their major concern; this is the case of the lining of nacelles in aircraft engine, or the lining of some test equipments like anechoic rooms. Acoustic absorption usually results from viscous and thermal phenomena at the interface between a structure and the fluid; it is improved by a suitable design of this interface. It may be tuned for a narrow frequency band (like in resonators [8,9]) or for broadband (like in porous or fibrous materials [10,11]). In any case, a major requirement is that the direct field of the source is not reflected at the interface, which must therefore ensure a fluid motion compatible with the incident pressure. A hidden requirement is also that the absorber structure (frame) must not vibrate, usually requiring to be installed on a stiff wall – although absorbing materials may be used to some extent with a limp frame configuration [12,13].

There are also applications requiring good performances both for absorption and transmission. Examples are compact machine hoods (for which the inside pressure must not increase too much as this would degrade the overall performance), and room acoustics where wall reflections must be controlled (*e.g.* to preserve speech intelligibility or the quality of musical events) while neighboring rooms require low background noise. A typical application could be a multiplex cinema, or a live music facility within an urban area. For such situations, the design must achieve both a low reflection coefficient on the source side (thus allowing suitable fluid motion) and a negligible motion of the wall on the receiver side. At first glance, it may seem that adding an absorbent layer to an existing wall would contribute to reduce the incident acoustic pressure on it, so leading to a reduction in transmission. This can be true only at higher frequencies, for which the inertia of the absorbing material frame is significant. At medium and lower

* Corresponding author.
E-mail address: manuel.melon@cnam.fr (M. Melon).

0003-682X/$ - see front matter © 2011 Elsevier Ltd. All rights reserved.
doi:10.1016/j.apacoust.2011.09.005

frequencies the viscous constraints are transmitted by the frame to the supporting wall. Moreover, acoustic absorption decreases with frequency, even for a very thick lining, and passive solutions thus reach their limits both for absorption and transmission.

Active control of sound has its maximum efficiency at low frequencies [14], so it has been used for direct active absorption and transmission control, especially for room acoustics for which it provides a mean to tune the acoustic behavior of the wall, and so to adjust it for different needs [15–18]. Many researchers have also proposed hybrid solutions where high frequencies are controlled by passive means while active components are used to reduce noise at low frequencies. Passive and active effects are then combined into a single hybrid cell. For instance, pressure release [19–21] or impedance matching methods [22–24] yielded to large absorption coefficients at low frequencies. Other authors [25–27] chose to embed the active component into the passive media to create smart foams. Active control has been widely used to reduce sound transmission, by controlling the vibration of a single panel [28,29], or through a smart foam [30]. A single actuator has been used for acting on a double panel [31,32]. Some authors also used two piezoelectric actuators bounded on the two sides of a double panel or two loudspeakers to improve the transmission loss of such walls [33–35].

Recently, Sitel et al. proposed to control simultaneously the absorption and the transmission of a hybrid cell involving a single actuator and several plates or layers of absorbing material [36]. The present paper extends this work by using two separate actuators for such a simultaneous control, and investigates the potential of the principle of this double-channel hybrid cell. This is based on a 1D model using the scattering matrix formalism. The system involves the single-DOF model of a dynamic loudspeaker which represents an active panel of finite stiffness (active structure). Its model is given by Section 2, and experimentally assessed in Section 3. Single and dual actuator cells are then simulated and compared in Section 4. Finally, in Section 5, results are discussed and evaluated with suggestions made for further research.

2. Component models

The purpose of this work is not to provide an accurate model, but to compare the dual-channel principle to previous ones. This section thus proposes a model as simple as possible, based on a circular cell which diameter is much smaller than the wavelength (LF approximation), fitted in an impedance tube which ensures normal incidence on the cell surface.

The dual-channel principle is investigated by considering a composite cell featuring two active structures and an absorbing plate, separated by air layers. The model of such a simple configuration may be obtained by the cascade of a few components, using the scattering matrix formalism which provides straightforwardly the reflection and transmission coefficients. Three components types are involved: air layer, porous layer, and finite stiffness active structures.

Following the above assumptions, a 1D behavior is assumed throughout this paper. Therefore each component of the module may each be described by a 2×2 scattering matrix $\mathbf{S_x^n}$ as follows:

$$\begin{Bmatrix} p_x^- \\ p_{x+l}^+ \end{Bmatrix} = \begin{bmatrix} S_{11}^n & S_{12}^n \\ S_{21}^n & S_{22}^n \end{bmatrix} \begin{Bmatrix} p_x^+ \\ p_{x+l}^- \end{Bmatrix}, \tag{1}$$

Note that +/− denotes propagation in the positive/negative x direction. The two indices x and $x + l$ here stand for two consecutive locations along the axis, while the n exponent expresses the nature of the considered component (air or porous layer, structure, etc.). Matrix entries S_{11}^n and S_{22}^n represent the anechoic reflection coefficients on each side of the component while S_{12}^n and S_{21}^n are the anechoic transmission coefficients.

As in a previous work [37], a simplified model is used to describe the behavior of a plate of finite stiffness, here considered as a single-degree-of-freedom structure as the frequency band of interest is usually close to the first flexural mode of the plate. Following the 1D approximation, this flexural mode is equivalent to a suspended piston of reduced equivalent area embedded into a rigid plate. The actuator technology is not the focus of the present work, so only its action on the equivalent normal displacement of the structure is considered here. The resulting component is then a two-port system as shown in Fig. 1, and its behavior can be expressed as follows:

$$\begin{pmatrix} p_a^- \\ p_b^+ \end{pmatrix} = \begin{bmatrix} S_{11}^s & S_{12}^s \\ S_{21}^s & S_{22}^s \end{bmatrix} \begin{pmatrix} p_a^+ \\ p_b^- \end{pmatrix} + \begin{pmatrix} p_s^- \\ p_s^+ \end{pmatrix}, \tag{2}$$

where p_a^+ and p_b^- are the incident pressure fields while p_a^- and p_b^+ are the pressure fields reflected by the structure. Whereas the scattering matrix $\mathbf{S^s}$ depicts its passive behavior, p_s^- and p_s^+ are the active pressures radiated under the influence of the embedded actuator.

2.1. Passive components

Within the simplified model considered in this paper, two components are passive ones: an air layer, and a layer of absorbing material. They are both described by symmetric scattering matrices thereafter.

With a $e^{j\omega t}$ dependence, the scattering matrix $\mathbf{S_x^a}$ of an air layer is given by

$$\begin{Bmatrix} p_x^- \\ p_{x+l_a}^+ \end{Bmatrix} = \begin{bmatrix} 0 & e^{-jkl_a} \\ e^{-jkl_a} & 0 \end{bmatrix} \begin{Bmatrix} p_x^+ \\ p_{x+l_a}^- \end{Bmatrix}. \tag{3}$$

where l_a is the thickness of the air layer. This matrix simply expresses the propagation delay of each of the travelling waves involved into the scattering matrix formulation.

The absorbing layer is here described as a plate made of porous media. To simplify the model, we choose to consider a porous media with rigid frame [10], leading to the following scattering matrix coefficients:

$$\begin{aligned} S_{11}^p = S_{22}^p &= \frac{j \sin k_m l_p \left(\frac{z_m}{\phi} - \frac{\phi}{z_m} \right)}{2 \cos k_m l_p + j \sin k_m l_p \left(\frac{z_m}{\phi} + \frac{\phi}{z_m} \right)}, \\ S_{12}^p = S_{21}^p &= \frac{2}{2 \cos k_m l_p + j \sin k_m l_p \left(\frac{z_m}{\phi} + \frac{\phi}{z_m} \right)}, \end{aligned} \tag{4}$$

where k_m and z_m are respectively the wave number and the reduced characteristic impedance of the porous media, while ϕ is its porosity and l_p its thickness. Parameters of the porous plate required by the Johnson–Allard Model [10] are: the flow resistivity σ, the porosity Φ, the tortuosity α_∞ and the viscous and thermal characteristic lengths Λ and Λ'. Their values are given in Table 1. Note that such a simple model can barely be accurate, as it assumes that the material

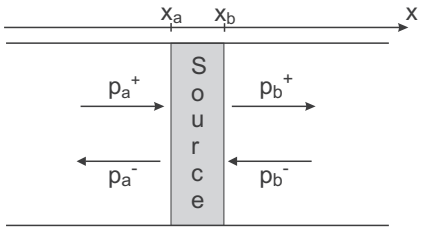

Fig. 1. Notation used for the active structure modelling.

Table 1
Parameters of the porous plate.

σ	Φ	α_∞	Λ	Λ'
20660 N m^{-4} s	0.99	1.01	45 μm	138 μm

frame is perfectly motionless, although there is a significant pressure difference between its two faces. This does however not prevent the analysis of the dual-channel control.

2.2. Active structure

As stated above, the active structure is reduced to a suspended piston (around its first resonance) with an equivalent axial actuator. The details of the actual geometry are not significant within the 1D and LF assumptions of this paper. The simplest experimental realization of such a simplified active structure is a rigid plate supporting an electrodynamic loudspeaker. We consider here a small compact loudspeaker featuring an inverted dome diaphragm and an external voice-coil. Its acoustic geometry is schematically shown in Fig. 2. Although the model presented here is based on this specific geometry, it can be applied to other loudspeakers with differing motor geometry, and the same approach could be used for other kind of actuators.

With the above assumptions, a lumped-element model describes adequately the finite stiffness of the structure and may be identified through acoustic measurements. This approach has been used to determine the classical Thiele/Small parameters commonly used for LF loudspeakers [38]. We therefore based our model on these parameters, with two extensions [39,40] which were found useful in a previous work [41]. This lumped-element model may however not be sufficient for our need as can be seen in Fig. 2, showing that the actual motor geometry modifies the effective area of the acoustic waveguide behind the loudspeaker. This may be even worse with more conventional drivers. Moreover, the actual diaphragm is not plane, and the resulting acoustic component cannot be considered a priori as a symmetric device. As in reference [37] this is taken into account in the scattering matrix by combining a rear acoustic load with the lumped-elements loudspeaker model. The model for the active structure is therefore built in two steps: a lumped-element model for the diaphragm and the motor, and then the rear acoustic load.

The behavior of the loudspeaker alone is expressed in terms of a scattering matrix $\mathbf{S}_\mathbf{x}^\mathbf{d}$ and an active pressure vector $\mathbf{p_U}$ (*cf.* Eq. (2)), considered between the two faces of the diaphragm (x_i close to x_b). The elements of $\mathbf{S}_\mathbf{x}^\mathbf{d}$ and $\mathbf{p_U}$ are expressed from the force balance equation applied to the loudspeaker moving mass and the electrical voltage U applied across the voice-coil, which lead to the following system of coupled equations:

$$\begin{cases} Bli = Z_m v_d + S_d\left(p_b^+ + p_b^-\right) - S_d\left(p_a^+ + p_a^-\right) \\ U = Z_e i + Bl v_d \end{cases}, \tag{5}$$

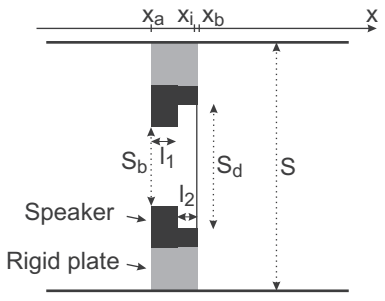

Fig. 2. Simplified geometry used for the loudspeaker modelling.

where Bl is the force factor, Z_e and Z_m are respectively the electrical and mechanical impedance of the moving assembly, i is the voice coil current, v_d is the moving mass velocity and S_d is the diaphragm radiating surface.

With Z_c denoting the characteristic impedance of air, the volume velocity conservation is given by

$$S_d v_d = S\frac{p_b^+ - p_b^-}{Z_c} = S_d\frac{p_i^+ - p_i^-}{Z_c}. \tag{6}$$

Determination of the diaphragm scattering matrix is achieved by performing the following steps:

- Voice coil current i is obtained from the second equation of system (5): $i = (U - Blv_d)/Z_e$.
- The second step consists in replacing i in the first equation of system (5).
- Expressing v_d in terms of $p_i^\pm$ and replacing it in the first equation of system (5) yields the determination of D_{11}, D_{12} and P_U^-. The last three entries (D_{21}, D_{22} and P_U^+) are obtained by expressing v_d in terms of $p_b^\pm$.
- Finally, the scattering matrix $\mathbf{S}_\mathbf{x}^\mathbf{d}$ and the active pressure $\mathbf{p_U}$ are respectively given by

$$\mathbf{S}_\mathbf{x}^\mathbf{d} = \begin{bmatrix} \dfrac{\xi - 1 + S_d/S}{\xi + 1 + S_d/S} & \dfrac{2}{\xi + 1 + S_d/S} \\ \dfrac{2}{(\xi+1)S/S_d + 1} & \dfrac{(\xi+1)S/S_d - 1}{(\xi+1)S/S_d + 1} \end{bmatrix}, \tag{7}$$

and

$$\mathbf{p_U} = \begin{pmatrix} p_U^- \\ p_U^+ \end{pmatrix} = \frac{BlU}{S_d Z_e}\begin{pmatrix} \dfrac{-1}{\xi + 1 + S_d/S} \\ \dfrac{1}{(\xi+1)S/S_d + 1} \end{pmatrix}, \tag{8}$$

where ξ, the reduced specific acoustic impedance of the diaphragm, is given by

$$\xi = \frac{1}{Z_c S_d}\left(Z_m + \frac{B^2 l^2}{Z_e}\right). \tag{9}$$

The lumped-elements model is then extended by a model of the acoustic circuit at the back of the membrane. As a rough approximation, the circuit between x_a and x_i can be described by two tubes of lengths l_1 and l_2 with respective surfaces S_b and S_d (see Fig. 2 and Table 2), leading to the scattering matrix

$$\begin{pmatrix} p_a^- \\ p_i^+ \end{pmatrix} = \begin{bmatrix} S_{11}^b & S_{12}^b \\ S_{21}^b & S_{22}^b \end{bmatrix}\begin{pmatrix} p_a^+ \\ p_i^- \end{pmatrix}. \tag{10}$$

where the expression for S_{ij}^b are given in Appendix A.

The global scattering matrix describing the active structure between x_a and x_b is then obtained from Eqs. (7), (8) and (10):

$$\mathbf{S}^\mathbf{s} = \begin{bmatrix} S_{11}^b + AS_{12}^b & BS_{12}^b \\ S_{21}^d(S_{21}^b + AS_{22}^b) & S_{22}^d + BS_{21}^d S_{22}^b \end{bmatrix}, \tag{11}$$

with

Table 2
Parameters of the loudspeaker's back acoustical circuit.

l_1	l_2	S_b
1.4 cm	1.2 cm	5.73 cm^2

$$A = \frac{S_{11}^d S_{12}^b}{1 - S_{11}^d S_{22}^b}$$
$$B = \frac{S_{12}^d S_{12}^b}{1 - S_{11}^d S_{22}^b} \quad (12)$$

The active pressure $\mathbf{p_s}$ is also modified by the rear acoustic load:

$$\begin{pmatrix} p_s^- \\ p_s^+ \end{pmatrix} = \begin{pmatrix} \dfrac{S_{12}^b}{1 - S_{11}^d S_{22}^b} p_U^- \\ p_U^+ + \dfrac{S_{22}^b S_{21}^d}{1 - S_{11}^d S_{22}^b} p_U^- \end{pmatrix}. \quad (13)$$

Eq. (13) shows that p_s^+ is the sum of the pressure p_U^+ radiated by the front side of the diaphragm and of a term which corresponds to the pressure radiated at the back, partially reflected by the rear load, and then transmitted through the membrane. Similarly p_s^- is the pressure radiated by the back of the membrane and transmitted through the rear load.

3. Active structure identification

As the active structure is the main component of the control cell and is described by a somewhat rough model, it cannot be used for simulation without first checking that its accuracy is adequate for the purpose of the paper. An experimental determination of the actual scattering matrix has thus been performed and is compared to the one computed from the proposed model.

3.1. Measurement set-up

The measurement method is derived from the work of Åbom et al. [42–44]. One advantage of this method is that it does not require an anechoic termination. The measurement set-up is shown in Fig. 3. As the two microphone method is known to give poor results when the microphone separation is close to half wavelength [45], four microphones are distributed on each side of the tested source. Eight transfer functions (microphone signal relative to electrical signal) are therefore recorded for each measurement. These measurements are carried out under three driving conditions, each involving a single active sound source while the two others are switched off. Measurements performed when driving one of the two external loudspeakers allow the determination of $\mathbf{S}^s$, while $\mathbf{p}_s$ is obtained from data obtained when driving the active structure, combined with the previously measured $\mathbf{S}^s$. More details on the method are given in Ref. [43].

The tube used for the measurements has a circular cross section with a 70 mm diameter. This method has been applied to the measurement of a 2″ Aura NSW2 loudspeaker (effective radiating diameter around 40 mm, as this device is relatively thin (see Table 2). The spacings between adjacent microphones are 5 cm, 15 cm and 25 cm. A band-limited white noise has been used for all measurement configurations.

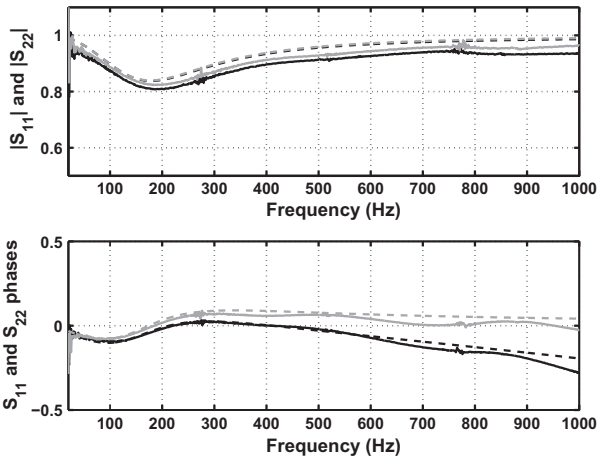

Fig. 4. Scattering matrix entries of the loudspeaker in short circuit. Upper graph: amplitude, lower graph: phase. Theoretical S_{11}^s (dashed black) and S_{22}^s (dashed gray), measured S_{11}^s (black) and S_{22}^s (gray).

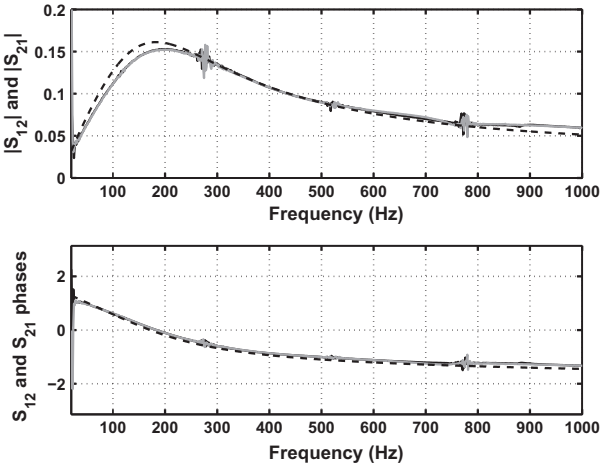

Fig. 5. Scattering matrix entries of the loudspeaker in short circuit. Upper graph: amplitude, lower graph: phase. Theoretical S_{12}^s (dashed black) and S_{21}^s (dashed gray), measured S_{12}^s (black) and S_{21}^s (gray).

3.2. Measurement results

Figs. 4 and 5 show a comparison of measured and computed $\mathbf{S}^s$ entries for the Aura loudspeaker with short-circuited voice-coil. The loudspeaker's parameters have been obtained classically from its electrical impedance measured under several conditions (loudspeaker alone, with an additional mass or mounted in a closed box). These parameters are given in Table 3.

Although the loudspeaker parameters have been obtained by an independent mean, the agreement between theoretical and measured values is fairly good. The mechanical resonance of the

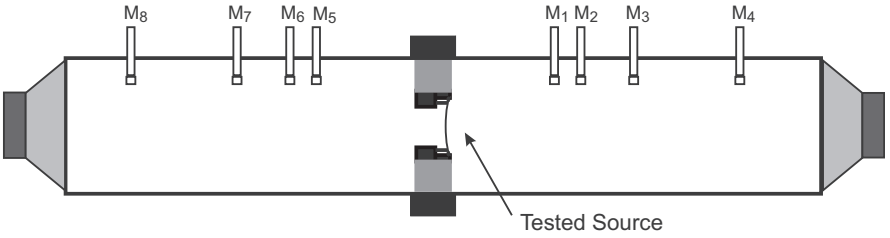

Fig. 3. Measurement set-up.

Table 3
Loudspeaker's parameters.

f_s = 173.6 Hz	$C_{ms} = 6.9 \times 10^{-4}$ m/N	M_{ms} = 1.22 g	Beta = 0.057 [39]
Q_{ms} = 4.78	R_e = 6.15 Ω	$K = 1.17 \times 10^{-3}$ [40]	$n = 0.812 \times 10^{-3}$ [40]
Q_{es} = 0.89	$S_d = 6.9 \times 10^{-4}$ m^2	$V_{as} = 1.535 \times 10^{-4}$ m^3	Bl = 3.03 T m

simulated active structure is around 180 Hz, a value compatible with a flexible plate of same dimension [36], but is much more damped as a result of the Laplace forces (electromagnetic damping). The difference in phase shifts for S^s_{11} and S^s_{22} reflects the non symmetric position of the diaphragm within the active structure, leading to a difference in propagation delays on both sides of the diaphragm. This is quite well predicted by the model including a rear acoustic load.

Results about the active pressure fields radiated by the Aura loudspeaker are shown in Fig. 6. The agreement between measured and predicted quantities is satisfactory although small discrepancies occur around driver resonance and at higher frequencies. Nevertheless, the model seems to provide a reasonable accuracy for the purpose of this paper. Note that above 300 Hz, the measurement of the pressure radiated at the back of the loudspeaker is slightly higher than the pressure radiated by the front of the membrane. This non symmetric behavior is common to many speaker geometries, and can be explained for this one by the rear acoustical load, which produces an Helmholtz resonance around 1850 Hz, thus increasing p_s^- relatively to p_s^+. This is not accurately predicted by our model, and will therefore be taken into account by an adjustable parameter $\kappa = p_s^-/p_s^+$ (for a perfectly symmetrical loudspeaker, $\kappa = -1$).

4. Simulations of hybrid cells

The components previously presented are used to simulate active control of absorption and transmission. The primary source is supposed to generate an incident wave coming from the positive side of the x axis, and an anechoic boundary condition is assumed in the negative direction ($p_a^+ = 0$). Denoting respectively "a" and "m" the starting and ending coordinates of the cell, the absorption coefficient is therefore defined as:

$$\alpha = 1 - |p_m^+/p_m^-|^2$$

and the transmission coefficient as:

$$T = |p_a^-/p_m^-|^2$$

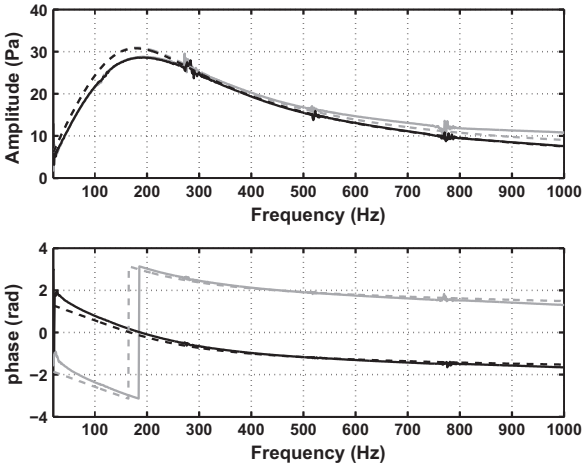

Fig. 6. Pressure radiated by the Aura loudspeaker. Theoretical p_s^+ (dashed black) and p_s^- (dashed gray), measured p_s^+ (black) and p_s^- (gray).

Ideal control of the cell acoustic transmission may then be achieved by driving it so that the transmitted pressure is zero, as could be monitored by a microphone located at a position $x \leqslant x_a$. Ideal control of the cell absorption would require a cardioid microphone located at a position $x \geqslant x_m$, but this is not a cheap sensor when dealing with lower frequencies. We therefore used the principle of pressure release control at the back of an absorbing layer [19–21].

Simulations are performed within a common frame for one and two active structures, and with and without active control. The active pressures radiated by the active structures are assumed not to be modified by other pressure fields, so that simulations may be computed as a superposition of passive and active situations. This may not be fully realistic, but allows to assess the interest of each active configuration, and to compare the simulated performances.

4.1. Single actuator system

The first configuration was already presented in a previous work [37], but with a different criterion for absorption control. It features an active structure separated from a relatively thin fibrous passive absorbent by a 2 cm air gap (see Fig. 7). This configuration is very typical of an hybrid (active/passive) absorbing cell.

The passive behavior of this cell is considered first. Fig. 8 plots the passive absorption and transmission coefficients, when the loudspeaker is short-circuited. Results show moderate absorption (<0.5) and insulation (≃10 dB) at low frequencies. In the considered frequency range, the 2″ Aura electrodynamic loudspeaker alone can be considered as a very simple mass/spring/damper mechanical system. Its transmission coefficient therefore exhibits a peak around its resonance frequency and decreases at lower frequencies (because of its stiffness) and at higher frequencies (because of its mass). An actual plate has a low damping, and thus exhibits a much narrower peak [36]. In our configuration, the loudspeaker features significant mechanical and electrodynamic damping, so its average passive transmission coefficient is low. Conversely, the loudspeaker is not well coupled to the air, so the major source of absorption in the hybrid system is the porous material, which performances are significant only at higher frequencies for the relatively thin layer considered here. The loudspeaker resonance is indeed providing some passive absorption at lower frequencies. This could be further improved by connecting a suitable shunt resistor [18], a quite simple and attractive solution. However this is restricted to a narrow frequency band, and may not provide the full benefit of adding a loudspeaker.

Considering now the active behavior, such a cell can be close to optimal for absorption. The porous plate is chosen with suitable values for its air resistivity σ and thickness l_p, so that $\sigma\ l_p = \rho_0 c$: the surface impedance of the porous plate is therefore equal to the characteristic impedance of air if the active structure ensures a pressure-release condition at the back of the porous plate. This can be obtained by driving it so as to cancel the pressure at location $x = x_c$, *ie* $p_c^+ = -p_c^-$. Using the above assumptions and Eqs. (1)–(4) yield the following reflection and transmission coefficients:

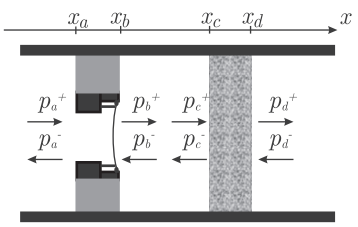

Fig. 7. Geometry of the single actuator cell with coordinates of sub-systems.

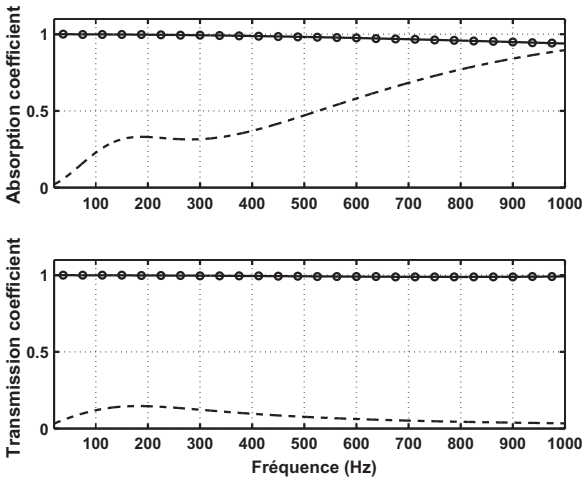

Fig. 8. Absorption coefficient (upper graph) and energetic transmission coefficient (lower graph) of the single actuator cell. Dashed lines: passive case, solid lines: active control).

$$R_c = \frac{p_d^+}{p_d^-} = S_{22}^p - \frac{S_{12}^p S_{21}^p}{1+S_{11}^p} = S_{11}^p - \frac{(S_{12}^p)^2}{1+S_{11}^p}, \tag{14}$$

and

$$T_c = \frac{p_a^-}{p_d^-} = \frac{S_{12}^p}{1+S_{11}^p}\left(S_{12}^s S_{12}^a - \kappa S_{22}^s S_{12}^a - \frac{\kappa}{S_{12}^a}\right). \tag{15}$$

The resulting active absorption coefficient is plotted in Fig. 8: it is very close to unity. There is a slight decrease at higher frequencies, as the porous media does not follow Darcy's law, even with the simplistic assumptions of our model: the porous plate surface impedance is thus not exactly σl_p. Active control of the absorption is however quasi-perfect over a wide frequency range, even with the simple criterion considered here.

Conversely, transmission losses are almost suppressed by the active control of absorption. This shows that the loudspeaker generates almost exactly the same volume velocity as the incident wave, and absorption thus results mostly from interference effects. This is consistent with a very low absorption by the porous plate, which thickness is optimized for active absorption.

The opposite behavior may be obtained by driving the active structure for maximum transmission loss, resulting however in reduced absorption. Several examples illustrating this trade-off can be found in a previous work [37]. It is worth noting that even when controlling for maximum absorption, the transmission losses are never worse than without the hybrid cell (there is no amplification of the transmitted wave). Simultaneous control of absorption and transmission may therefore be considered, but cannot be optimal without a dual-channel system.

4.2. Dual actuator system

The dual-channel configuration makes use of two identical active structures, as shown in Fig. 9. Note that one loudspeaker is flipped left to right. The porous layer is the same as for the previous configuration, and the two air gaps have the same 2 cm thickness.

The right active structure is driven similarly to the previous cell, to achieve the pressure release condition $p_e^+ = -p_e^-$. In addition, the left active structure is driven in order to cancel the transmitted pressure: $p_a^- = 0$. The cell then features two active structures driven from two microphone outputs, so its simulation requires a matrix inversion. For the simple case considered here, an analytical solution can be obtained, and is given in Appendix B.

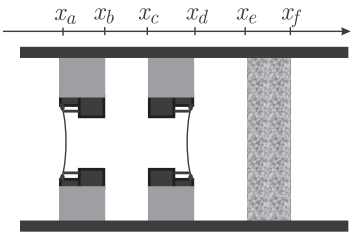

Fig. 9. Geometry of the dual actuator cell with coordinates of sub-systems.

The corresponding results are shown in Fig. 10: the proposed system can indeed deal simultaneously with both absorption and insulation. This result is no surprise as our simulation is based on the superposition of the two control situations. More interesting is the computation of the radiated pressures required by the control for each loudspeaker, which are plotted in Fig. 11.

The left structure radiates p_{s1}^+ which is very low above 400 Hz, but can exceed the incident pressure below 120 Hz. The right structure radiates p_{s2}^+ which amplitude is close to the incident one, except below 200 Hz for which p_{s2}^+ rises significantly. This results from the interference between the two loudspeakers: as their passive transmission loss is relatively low, each one produces a non-negligible pressure on the microphone which monitors the opposite control channel, and part of the control effort is wasted in self-cancellation of the two active structures. This remains however within reasonable values for the considered cell.

5. Discussion

The behavior of the dual-channel hybrid cell may be investigated by computing the matrix transfer function between the voltages feeding the loudspeakers (U in Eq. (5)) and the two pressures p_e and p_a^-. The variations with frequency of its condition number $\mathcal{C}$ are presented in Fig. 12 (dashed black line, for $\kappa = -1.0$). $\mathcal{C}$ remains close to 2, except at lower frequencies for which it raises significantly, as a result of the interference between both radiating structures.

The practical consequence of this interference is the voltage required to drive the two loudspeakers, presented in Fig. 13. As could be expected, it is increased at lower frequencies for both loudspeakers. The required values are however still reasonable, and can be further reduced by taking advantage of the natural asymmetry of actual speakers (as noticed on measurements in Section

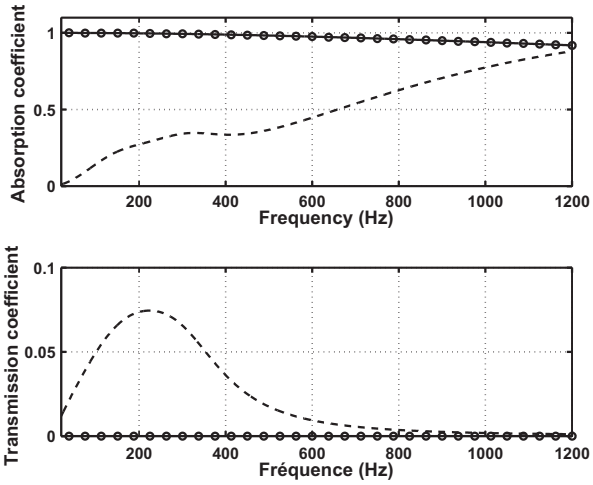

Fig. 10. Absorption coefficient (upper graph) and energetic transmission coefficient (lower graph) of the dual actuator cell. Dashed lines: passive case, solid lines: active control).

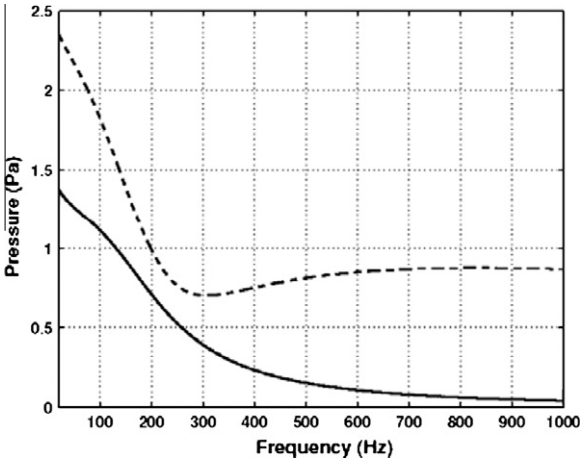

Fig. 11. Modules of the pressure radiated by the loudspeakers: p_{s1}^{+}: solid line, p_{s2}^{+}: dashed line.

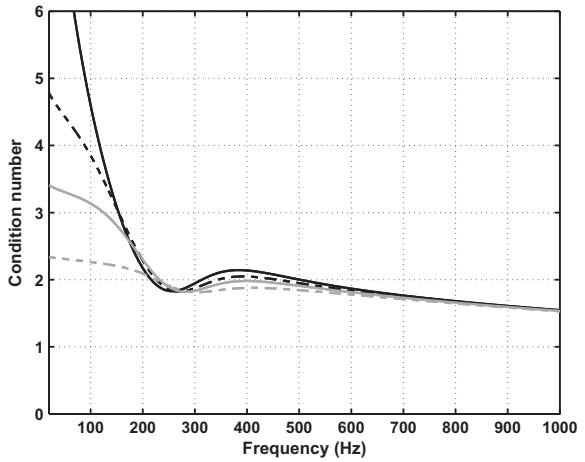

Fig. 12. Condition number of the cell transfer matrix. Solid lines: $\kappa = -1.2$, dashed lines: $\kappa = -1.0$, solid gray lines: $\kappa = -0.83$ and dashed gray lines: $\kappa = -0.5$.

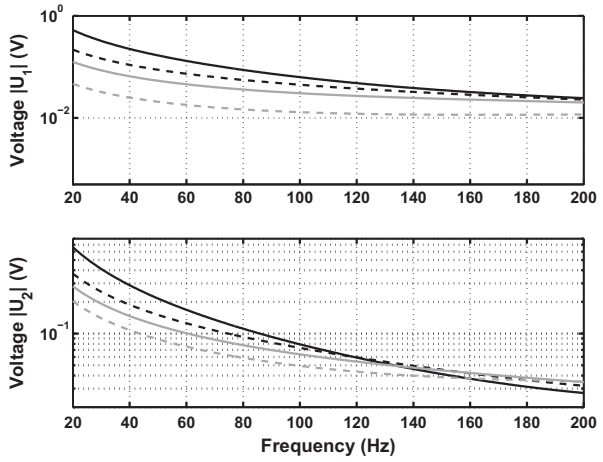

Fig. 13. Modules of the voltage applied to the loudspeakers, left loudspeaker (upper graph) and right loudspeaker (lower graph). Solid lines: $\kappa = -1.2$, dashed lines: $\kappa = -1.0$, solid gray lines: $\kappa = -0.83$ and dashed gray lines: $\kappa = -0.5$.

3.2). This is investigated by varying arbitrarily the directivity factor κ which reflects the geometry of the loudspeaker: ($\kappa = -1$ for a perfectly symmetric loudspeaker and $\kappa = 0$ for a cardioid source). Although values very different from unity are not common for commercial devices, it could be tailored to a specific (reasonable) value if required. We restricted ourselves to values of -1 and -0.5, which we expect to be compatible with usual manufacturing processes. We also used a value of -0.83 and -1.2 which correspond respectively to the maximum measured experimental asymmetry (*cf.* Fig. 5 around 1 kHz) and to the same loudspeaker fitted with a reverse orientation. Results are plotted in Fig. 13. Between 20 and 200 Hz, voltages are significantly reduced for $\kappa = -0.5$, e.g. by a factor of about 4 for the left loudspeaker and about 2 for the right loudspeaker at 50 Hz. Moreover, condition number $\mathcal{C}$ at low frequencies decreases (Fig. 12) when interferences between sources are reduced. These results show the interest to achieve even a modest imbalance between front and rear pressure radiation.

The model presented here could be used to simulate more sophisticated configurations, *e.g.* involving more layers. We did not consider this worthy because such an 1D study already lacks many effects, especially compared to a realistic 3D situation. We believe that the presented model, backed by the experimental assessment of the active structure model, can speed up the design of an actual cell mock-up, at least at a preliminary stage. The main results are:

The possibility to use dual-channel local controller from two pressure measurements, for simultaneous control of absorption and transmission.
The importance of the passive transmission losses of the active structures for the conditioning of the problem.
The interest to use the natural asymmetry of loudspeaker for improving the efficiency of the cell.

A practical implementation would however need to solve many issues, including the manufacturing of such asymmetric active structure, and the signal reference for the control (for a feedforward implementation) or its stability (for a feedback implementation). These are far beyond the scope of the present work, and will be investigated as part of an ongoing research project.

Acknowledgment

This work has been supported by the French National Research Agency (ANR: Agence nationale de la recherche) as part of the PARABAS project (ANR-06-BLAN-0081).

Appendix A. Loudspeaker's back scattering matrix

The scattering matrix $\mathbf{S^b}$ of the loudspeaker's back can be easily calculated from its transfer matrix $\mathbf{T_b}$ which is given by $\mathbf{T^b} = \mathbf{T^{con}} \cdot \mathbf{T^{l_1}} \cdot \mathbf{T^{exp}} \cdot \mathbf{T^{l_2}}$ [46] where $\mathbf{T^{l_{1,2}}}$ are the transfer matrices of the tubes given by

$$\mathbf{T^{l_{1,2}}} = \begin{bmatrix} \cos(kl_{1,2}) & jZ_c.\sin(kl_{1,2}) \\ j\sin(kl_{1,2})/Z_c & \cos(kl_{1,2}) \end{bmatrix}, \tag{A.1}$$

while $\mathbf{T^{con}}$ and $\mathbf{T^{exp}}$ respectively are the transfer matrices of the sudden area discontinuities (contraction and expansion) and are given by

$$\mathbf{T^{con}} = \begin{bmatrix} 1 & 0 \\ 0 & S_b/S \end{bmatrix} \tag{A.2}$$

and

$$\mathbf{T^{exp}} = \begin{bmatrix} 1 & 0 \\ 0 & S_d/S_b \end{bmatrix}. \tag{A.3}$$

Relations between scattering and transfer matrices yields

$$\mathbf{S^b} = \begin{bmatrix} \dfrac{X^+ - W^+}{X^+ + W^+} & \dfrac{W^+X^- - X^+W^-}{X^+ + W^+} \\ \dfrac{2}{X^+ + W^+} & \dfrac{-X^- + W^-}{X^+ + W^+} \end{bmatrix}, \tag{A.4}$$

with

$$\begin{cases} X^{\pm} = T^b_{11} \pm T^b_{12}/Z_c \\ W^{\pm} = T^b_{21} Z_c \pm T^b_{22} \end{cases} \tag{A.5}$$

Appendix B. Radiated pressure fields

For the dual actuator system, radiated pressure fields in the controlled situation can be calculated by using scattering matrices of the sub-systems. The incident and reflected pressure fields on the left loudspeaker are given by

$$\begin{pmatrix} p_a^- \\ p_b^+ \end{pmatrix} = \begin{bmatrix} S^s_{22} & S^s_{12} \\ S^s_{12} & S^s_{11} \end{bmatrix} \begin{pmatrix} p_a^+ \\ p_b^- \end{pmatrix} + \begin{pmatrix} -p^+_{s1} \\ -\kappa p^+_{s1} \end{pmatrix}. \tag{B.1}$$

Note that coefficients have been switched (and negated for active parts) to take into account the speaker's orientation. For the right loudspeaker, the behavior equations are given by

$$\begin{pmatrix} p_c^- \\ p_d^+ \end{pmatrix} = \begin{bmatrix} S^s_{11} & S^s_{12} \\ S^s_{12} & S^s_{22} \end{bmatrix} \begin{pmatrix} p_c^+ \\ p_d^- \end{pmatrix} + \begin{pmatrix} \kappa p^+_{s2} \\ p^+_{s2} \end{pmatrix}. \tag{B.2}$$

The left air layer behavior is described by Eq. (3) while the right one is described by the following equation:

$$\begin{Bmatrix} p_d^- \\ p_e^+ \end{Bmatrix} = \begin{bmatrix} 0 & S^a_{12} \\ S^a_{12} & 0 \end{bmatrix} \begin{Bmatrix} p_d^+ \\ p_e^- \end{Bmatrix}. \tag{B.3}$$

The porous plate can be modelized by the following set of equations:

$$\begin{Bmatrix} p_e^- \\ p_f^+ \end{Bmatrix} = \begin{bmatrix} S^p_{11} & S^p_{12} \\ S^p_{12} & S^p_{22} \end{bmatrix} \begin{Bmatrix} p_e^+ \\ p_f^- \end{Bmatrix}. \tag{B.4}$$

Using Eqs. (B.1)–(B.4) and (3), anechoic assumption in the negative direction ($p_a^+ = 0$) and control conditions ($p_a^- = 0$ and $p_e^- + p_e^+ = 0$) yield the following radiated pressure expressions for $p_6^- = 1$ Pa.

$$\begin{cases} p^+_{s2} = \dfrac{S^s_{11} D - D/C - \left(S^s_{12} S^a_{12}\right)^2}{1/C + \kappa/S^s_{12} - S^s_{11}} \dfrac{S^p_{12}}{S^a_{12}\left(1 + S^p_{11}\right)}, \\ p^+_{s1} = \dfrac{D S^s_{12} S^p_{12}}{C\left(1 + S^p_{11}\right)} + \dfrac{S^a_{12}}{C} p^+_{s2}, \end{cases} \tag{B.5}$$

with

$$\begin{cases} C = \left(S^a_{12}\right)^2 \left(S^s_{11} - \kappa S^s_{12}\right) \\ D = 1 + S^s_{22}\left(S^a_{12}\right)^2 \end{cases}. \tag{B.6}$$

References

[1] Brouard B, Lafarge D, Allard J-F. A general method of modelling sound propagation in layered media. J Sound Vib 1995;183(1):129–42.
[2] Lee F-C, Chen W-H. Acoustic transmission analysis of multi-layer absorbers. J Sound Vib 2001;248(4):621–34.
[3] Zhu CY, Huang Q. A method for calculating the absorption coefficient of a multi-layer absorbent using the electro-acoustic analogy. Appl Acoust 2005;66(7):879–87.
[4] Zulkifli R, Nor MJM, Tahir MFM, Ismail AR, Nuawi MZ. Acoustic properties of multi-layer coir fibres sound absorption panel. J Appl Sci 2008;8(20):3703–14.
[5] Jean P, Rondeau J-F. A simple decoupled modal calculation of sound transmission between volumes. Acta Acust United Acust 2002;88(6):924–33.
[6] Guigou-Carter C, Villot M. Modelling of sound transmission through lightweight elements with stiffeners. Build Acoust 2003;10(3):193–209.
[7] Jean P, Siwiak H, Joubert G. A decoupled vibro-acoustic development of FEM: application to laboratory modelling. Build Acoust 2006;13(2):83–98.
[8] Sapoval B, Haeberlé O, Russ S. Acoustical properties of irregular and fractal cavities. J Acoust Soc Am 1997;102(4):2014–9.
[9] Kim HJ, Cha J-P, Song J-K, Ko YS. Geometric and number effect on damping capacity of Helmholtz resonators in a model chamber. J Sound Vib 2010;329(16):3266–79.
[10] Allard J-F. Propagation of sound in porous media: modelling sound absorbing materials. Elsevier; 1993.
[11] Allard JF, Atalla N. Propagation of sound in porous media: modelling sound absorbing materials. 2nd ed. Wiley; 2009.
[12] Doutres O, Dauchez N, Génevaux J-M, Dazel O. Validity of the limp model for porous materials: a criterion based on the Biot theory. J Acoust Soc Am 2007;122(4):2038–48.
[13] Panneton RE. Comments on the limp frame equivalent fluid model for porous media. J Acoust Soc Am 2007;122(6):EL217.
[14] Nelson PA, Elliott SJ. Active control of sound. Academic Press; 1991.
[15] Lissek H, Meynial X. A preliminary study of an isodynamic transducer for use in active acoustic materials. Appl Acoust 2003;64(9):917–30.
[16] Zhu H, Rajamani R, Stelson KA. Active control of acoustic reflection, absorption, and transmission using thin panel speakers. J Acoust Soc Am 2003;113(2):852–70.
[17] Boulandet R, Lissek H. Optimization of electroacoustic absorbers by means of designed experiments. Appl Acoust 2010;71(9):830–42.
[18] Lissek H, Boulandet R, Fleury R. Electroacoustic absorbers: bridging the gap between shunt loudspeakers and active sound absorption. J Acoust Soc Am 2011;129(5).
[19] Thenail D, Galland M-A, Sunyach M. Active enhancement of the absorbent properties of a porous material. Smart Mater Struct 1994;3:18–25.
[20] Furtoss M, Thenail D, Galland M-A. Surface Impedance control for sound absorption: direct and hybrid passive/active strategies. J Sound Vib 1997;203(2):219–36.
[21] Sellen N, Cuesta M, Galland M-A. Noise reduction in a flow duct: implementation of a hybrid passive/active solution. J Sound Vib 2006;297(3-5):492–511.
[22] Beyene S, Burdisso RA. A new hybrid passive–active noise absorption system. J Acoust Soc Am 1997;101(3):1512–5.
[23] Smith J, Johnson BD, Burdisso RA. A broadband passive–active sound absorption system. J Acoust Soc Am 1999;106(5):2646–52.
[24] Cobo P, Pfretzschner J, Cuesta M, Anthony DK. Hybrid passive–active absorption using microperforated panels. J Acoust Soc Am 2004;116(4):2118–25.
[25] Guigou C, Fuller CR. Control of aircraft interior broadband noise with foam-PVDF smart skin. J Sound Vib 1999;220(3):541–57.
[26] Leroy P, Atalla N, Berry A, Herzog Ph. Three dimensional finite element modeling of smart foam. J Acoust Soc Am 2009;126(5):2873–85.
[27] Leroy P, Berry A, Herzog Ph, Atalla N. Experimental study of a smart foam sound absorber. J Acoust Soc Am 2011;129(1):154–64.
[28] Henry JK, Clark RL. Active control of sound transmission through a curved panel into a cylindrical enclosure. J Sound Vib 2002;249(2):325–49.
[29] Chen K, Li S, Hu H, Lu J. Some physical insights for active acoustic structure. Appl Acoust 2009;70(6):875–83.
[30] Kundu A, Berry A. Active control of transmission loss with smart foams. J Acoust Soc Am 2011;129(2):726–40.
[31] Leishman TW, Tichy J. A theoretical and numerical analysis of vibration-controlled modules for use in active segmented partitions. J Acoust Soc Am 2005;118(3):1424–38.
[32] Hu Y, Sitel A, Galland M-A, Chen K. A plane wave study for improving acoustical performance of double wall systems using an active–passive method. Noise Contr Eng J 2009;57(3):193–202.
[33] Carneal JP, Fuller CR. An analytical and experimental investigation of active structural acoustic control of noise transmission through double panel systems. J Sound Vib 2004;272(3–5):749–71.
[34] Sagers JD, Leishman TW, Blotter J. A double-panel active segmented partition module using decoupled analog feedback controllers: numerical model. J Acoust Soc Am 2009;125(6):3806–18.
[35] Sagers JD, Leishman TW, Blotter J. Active sound transmission control of a double-panel module using decoupled analog feedback control: experimental results. J Acoust Soc Am 2010;128(5):2807–16.
[36] Sitel A, Galland M-A. Scattering matrix formulation for both measurement and prediction of acoustical performances of hybrid cells and their active and passive elements. Acta Acust United Acust, in press.
[37] Melon M, Sitel A, Galland MA, Herzog Ph. Measurement of a loudspeaker transfer matrix for hybrid active/passive absorbers. In: Proc ACTIVE 2009 CD:AC09-805, Ottawa; 2009.
[38] Anderson BE, Leishman TW. An acoustical measurement method for the Derivation of loudspeaker parameters. In: 115th Conv Audio Eng Soc paper 5965, New York; 2003.
[39] Knudsen JG, Jensen MH. Low-frequency loudspeaker models that include suspension creep. J Audio Eng Soc 1993;41(1–2):3–18.
[40] Leach W. Loudspeaker voice-coil inductance losses: circuit models, parameter estimation and effect on frequency response. J Audio Eng Soc 2002;50(6):442–50.
[41] Melon M, Langrenne Ch, Herzog Ph, Garcia A. Evaluation of a method for the measurement of subwoofers in usual rooms. J Acoust Soc Am 2010;127(1):256–63.
[42] Åbom M. Measurement of the scattering matrix of acoustical two-ports. Mech Syst Sig Proc 1991;5(2):89–104.

[43] Lavrenjev J, Åbom M, Bodén H. A measurement method for determinining the source data of acoustic two-port sources. J Sound Vib 1995;197(1):516–31.
[44] Åbom M. A note on the experimental determination of acoustical two-port matrices. J Sound Vib 1992;155(1):185–8.
[45] Bodén H, Åbom M. Influence of errors on the two-microphone method for measuring acoustic properties in ducts. J Acoust Soc Am 1985;79(2):541–9.
[46] Munjal ML. Acoustics of ducts and mufflers. John Wiley & Sons; 1987.